

ISO LWS SPECTROSCOPY OF M82: A UNIFIED EVOLUTIONARY MODEL

JAMES W. COLBERT,^{1,2} MATTHEW A. MALKAN,¹ PETER E. CLEGG,³ PIERRE COX,⁴ JACQUELINE FISCHER,⁵ STEVEN D. LORD,⁶
MICHAEL LUHMAN,^{5,7} SHOBITA SATYAPAL,^{8,9} HOWARD A. SMITH,¹⁰ LUIGI SPINOGLIO,¹¹ GORDON STACEY,¹² AND
SARAH J. UNGER³

Received 1998 May 29; accepted 1998 September 4

ABSTRACT

We present the first complete far-infrared spectrum (43–197 μm) of M82, the brightest infrared galaxy in the sky, taken with the Long Wavelength Spectrometer of the *Infrared Space Observatory* (ISO). We detected seven fine structure emission lines, [O I] 63 and 145 μm , [O III] 52 and 88 μm , [N II] 122 μm , [N III] 57 μm , and [C II] 158 μm , and fitted their ratios to a combination starburst and photo-dissociation region (PDR) model. The best fit is obtained with H II regions with $n = 250 \text{ cm}^{-3}$, an ionization parameter of $10^{-3.5}$, and PDRs with $n = 10^{3.3} \text{ cm}^{-3}$ and a far-ultraviolet flux of $G_0 = 10^{2.8}$. We applied both continuous and instantaneous starburst models, with our best fit being a 3–5 Myr old instantaneous burst model with a 100 M_\odot cutoff. We also detected the ground-state rotational line of OH in absorption at 119.4 μm . No excited level OH transitions are apparent, indicating that the OH is almost entirely in its ground state with a column density $\sim 4 \times 10^{14} \text{ cm}^{-2}$. The spectral energy distribution over the long-wavelength spectrometer wavelength range is well fitted with a 48 K dust temperature and an optical depth, $\tau_{\text{Dust}} \propto \lambda^{-1}$.

Subject headings: dust, extinction — galaxies: individual (M82) — galaxies: ISM — galaxies: starburst — infrared: galaxies

1. INTRODUCTION

Infrared luminous galaxies emit an infrared luminosity comparable to or greater than their optical luminosity. The starburst galaxy is an infrared luminous galaxy converting its molecular interstellar medium (ISM) into stars at a rate that can not be sustained for a Hubble time. The radiation from these new stars is reprocessed into infrared radiation by the dust in their parental molecular clouds. Other possible energy sources for infrared luminous galaxies are active galactic nuclei or the energy of shocks resulting from galaxy interactions. Recent studies (e.g., Genzel et al. 1998) support the hypothesis that most of the brightest infrared luminous galaxies are predominantly powered by recently formed massive stars; however, the simultaneous presence of active galactic nuclei and active star formation in some galaxies shows that both processes can occur in the same phase of the evolution of luminous infrared galaxies.

As a result of its proximity (3.63 Mpc; Freedman et al. 1994) and moderate infrared luminosity, M82 is the brightest galaxy in the infrared. Because of its recent episode of star formation (e.g., Rieke et al. 1993), it is considered to be

the prototypical starburst galaxy. Sometime around 10^8 yr ago, M82 experienced a close encounter with M81 (Yun, Ho, & Lo 1993). This gravitational interaction likely produced the bar seen (Telesco et al. 1991), which provided the large streaming motions necessary to funnel large amounts of molecular gas to the galaxy's center. This large reservoir of molecular gas, $\sim 2 \times 10^8 M_\odot$ (Wild et al. 1992), provides the fuel for the ongoing starburst.

Studies of the M82 nucleus in the mid-infrared (Telesco et al. 1991) saw strong off-center hot spots. Using the velocity profiles of the M82 far-infrared fine structure lines, Lord et al. (1996) modeled two hot spots as well. These hot spots may be star formation sites resulting from cloud-cloud collisions that occur because of orbital crowding near the inner Lindblad resonances (Kenney et al. 1992). Alternatively, Satyapal et al. (1997) modeled the nucleus of M82 as a region of outward star propagation, with the hot spots being the most recent and brightest areas of star formation.

Relatively insensitive to extinction, far-infrared spectroscopy can provide a unique probe of infrared-bright, dust-obscured galaxies like M82. Line ratios may be used to constrain physical parameters and tend to be less vulnerable to calibration uncertainties as well. It is also in the far-infrared that some of the most important cooling lines of the ISM of galaxies, the [O I] 63 μm and [C II] 158 μm lines, appear. A close examination of M82 will provide a template for future comparisons to possible starburst galaxies, including those at high redshift.

Our observations and the analysis used on the M82 far-infrared spectrum are described in § 2, and § 3 presents our fine structure line results. We discuss line ratio model fitting, OH absorption, and fitting of the entire spectrum in § 4; § 5 presents our final conclusions.

2. OBSERVATIONS AND ANALYSIS

We present *Infrared Space Observatory* (ISO) long-wavelength spectrometer (LWS; Kessler et al. 1996; Clegg et al. 1996) grating mode (43–196.7 μm , $\lambda/\Delta\lambda \sim 200$) observations of M82. These observations were taken as part of

¹ Department of Physics and Astronomy, University of California, Los Angeles, CA 90095.

² Email: colbert@astro.ucla.edu.

³ Physics Department, Queen Mary and Westfield College, University of London, Mile End Road, London E1 4NS, England, UK.

⁴ Institut d'Astrophysique Spatiale, Bâtiment 120, Université de Paris XI, F-91405 Orsay, France.

⁵ Naval Research Laboratory, Remote Sensing Division, 4555 Overlook Avenue SW, Washington, DC 20375.

⁶ Infrared Processing and Analysis Center, California Institute of Technology, Pasadena, CA 91125.

⁷ NRC-NRL Research Associate.

⁸ Goddard Space Flight Center, Code 685, Greenbelt, MD 20771.

⁹ NRC-NASA Research Associate.

¹⁰ Harvard-Smithsonian Center for Astrophysics, 60 Garden Street, Cambridge, MA 02138.

¹¹ CNR-Istituto di Fisica dello Spazio Interplanetario, CP 27, 00044 Frascati, Italy.

¹² Department of Astronomy, 510 Space Science Building, Cornell University, Ithaca, NY 14853.

the Long Wavelength Spectrometer Consortium's Extragalactic Guaranteed-Time Program. All observations were made in 1996 May on two separate orbits. The central position was R.A. (2000) = $9^{\text{h}}55^{\text{m}}52^{\text{s}}.3$ and decl. (2000) = $69^{\circ}40'45''.9$. Our main observations consisted of 20 full grating scans, with a total integration over all scans of 8 s at each wavelength position spaced at one-quarter of the resolution element. The spectral resolution was $0.29 \mu\text{m}$ for the 43–93 μm range and $0.6 \mu\text{m}$ for the 80–196 μm range. Also, in the final averaged spectrum, the spectral resolution between 80 and 93 μm lies between these two values, resulting from our averaging of the overlap of two detectors that are detecting different orders of the grating. We also took a spectrum offset by $\Delta\alpha = +0^{\circ}.8$ and $\Delta\delta = +17'$ from the center of the galaxy in order to measure the background. This offset observation had the same integration time but was over a more limited wavelength range. All data used in this paper were processed through the LWS Pipeline Version 7.

The spectra were flux-calibrated with respect to Uranus (Swinyard et al. 1998). The individual detector scans were calibrated to within $\pm 4\%$ – 6% of each other, based on overlapping detectors, with the notable exception of detector LW4, covering wavelengths 150–170 μm , about 15% lower. Several reliable detectors were chosen, and the rest of the detectors were multiplicatively shifted so that overlapping points would match. The LWS beam is roughly $80''$ FWHM, but it does show some variation with detector, ranging from $65''$ – $85''$ FWHM (Swinyard et al. 1998).

We performed the postpipeline analysis with the ISO Spectral Analysis Package (ISAP). Even after pipeline processing the spectrum remains contaminated with bad data point “glitches” from cosmic ray hits, which we cleaned by plotting several scans on top of each other and looking for the characteristic fast rising and slowly falling glitch shape. All bad data points were then removed as well as any suspicious and widely deviating points following the glitch, where the detector showed memory effects. Roughly 20% of the data were discarded as unusable.

Raw data also contain a fringing pattern that is believed to arise from interference between the beam coming off the field mirror and another beam reflected by the substrate holding that mirror. Fringing is only a minor effect for the shorter wavelengths ($< 70 \mu\text{m}$): the fringing is weaker, and the spectrum is inherently noisier. At wavelengths longer than 100 μm , fringes approach $\sim 5\%$ of the continuum and endanger our ability to measure accurately the continuum level as well as to identify possible weak emission and absorption lines. The fringe is sinusoidal in wavenumber

with a well-measured period of 3.54 cm^{-1} . We used the sine-wave-fitting algorithm for extended sources in ISAP to divide out the fringes. The defringing has little effect on the majority of line fluxes, altering the weak 145 and 122 μm lines by only 5%. Only the OH absorption at 119 μm changes significantly, becoming 33% weaker. Finally, we used a 3σ median clip on the data before averaging it all into a single spectrum with bins of $0.05 \mu\text{m}$.

3. FINE STRUCTURE EMISSION LINES

Table 1 lists the seven fine structure lines detected along with 1σ uncertainties. The measured wavelength of each line is consistent with a 225 km s^{-1} redshift. The τ 's listed are optical depths at each wavelength assuming a dust extinction model from Adams, Lada, & Shu (1988) and $\tau_{\lambda} \propto \lambda^{-1}$ at wavelengths longer than $\sim 50 \mu\text{m}$. We calibrate this model using the visual extinction from the study of near-infrared hydrogen recombination lines by Satyapal et al. (1995). Assuming a foreground screen they found an A_V that ranged from 2–12 mag, with its highest values near the nucleus where $A_V \sim 10$. We adopt this central value of 10 for our visual extinction, noting that at the wavelengths we are considering small errors in A_V have little effect on the final line fluxes. The corrected flux is the measured flux multiplied by $\exp(\tau)$, appropriate for an external dust screen. Figure 1 displays the entire spectrum.

The fine structure lines we present have been measured in the past by the Kuiper Airborne Observatory (KAO; Lord et al. 1996; Petuchowski et al. 1994; Stacey et al. 1991; Duffy et al. 1987; Lugten et al. 1986; Watson et al. 1984), but most were taken on separate nights with different calibrators. This complicates line ratios, because beam sizes, spectral resolutions, and flux calibration schemes differ. Another advantage of this spectrum over KAO is the complete absence of telluric absorption features, which had greatest effect on the measurements of the [O I] 63 μm and [N II] 122 μm lines. We have improved the signal-to-noise ratio on all lines, but the greatest increases were for the weak [N II] 122, [N III] 57, and [O I] 145 μm lines. Table 2 gives the KAO lines and their measured continuum. Several of the KAO continuum measurements provided are published here for the first time.

The agreement between the KAO measurements and our own fluxes is satisfactory, with the most significant differences in the weak [N II] 122 and [O I] 145 μm lines. Our continuum measurements, however, go from being 30% higher to 10% lower than the KAO values. Some of this may be due to the smaller beams employed for KAO work (30"–55"), but that cannot explain all the discrepancies.

TABLE 1
EMISSION-LINE FLUXES

Line	Rest λ (μm)	Flux (W cm^{-2})	τ	Corrected Flux (W cm^{-2}) ^a	Continuum (Jy) ^b
[O III].....	51.81	$10.3 \pm 0.5 \times 10^{-18}$	0.10	$11.3 \pm 0.6 \times 10^{-18}$	1490
[N III].....	57.32	$3.4 \pm 0.5 \times 10^{-18}$	0.09	$3.7 \pm 0.5 \times 10^{-18}$	1695
[O I].....	63.18	$17.6 \pm 0.5 \times 10^{-18}$	0.08	$19.1 \pm 0.5 \times 10^{-18}$	1860
[O III].....	88.36	$8.6 \pm 0.4 \times 10^{-18}$	0.06	$9.1 \pm 0.4 \times 10^{-18}$	1970
[N II].....	121.90	$1.7 \pm 0.3 \times 10^{-18}$	0.04	$1.8 \pm 0.3 \times 10^{-18}$	1460
[O I].....	145.53	$1.2 \pm 0.1 \times 10^{-18}$	0.04	$1.2 \pm 0.1 \times 10^{-18}$	1155
[C II].....	157.74	$13.4 \pm 0.1 \times 10^{-18}$	0.03	$13.8 \pm 0.1 \times 10^{-18}$	1005

^a Corrected flux is the measured flux corrected for extinction.

^b Continuum flux density has not been corrected for extinction.

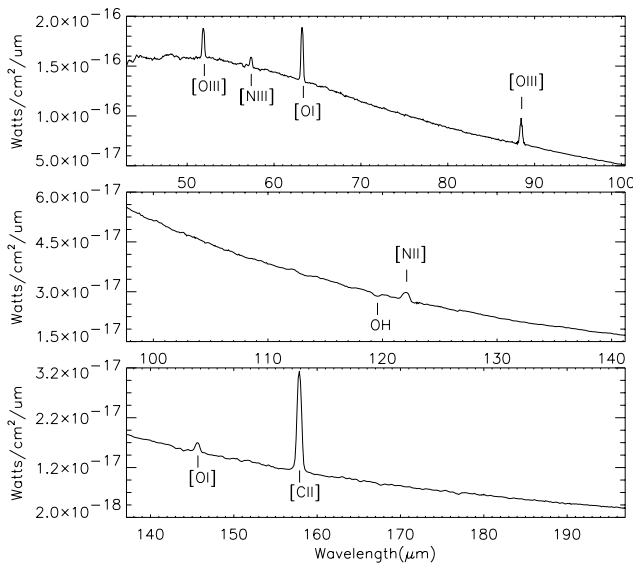


FIG. 1.—LWS spectrum for M82. Seven fine structure lines are visible, as well as an OH absorption at 119 μm . The strong features seen around 43–50 μm are unidentified and possibly artifacts of the first detector.

The *Infrared Astronomical Satellite (IRAS)* measured a continuum flux of 1271 Jy at 60 μm and 1351 Jy at 100 μm (Rice et al. 1988), both lower measurements than those presented here. Since the *IRAS* values represent the total M82 flux in an area roughly $10' \times 5'$ and since the background measured by *IRAS* and by us in reference positions is less than 2 Jy, the reason for this discrepancy is unknown.

While the previous line work (Duffy et al. 1987; Lugten et al. 1986; Lord et al. 1996) achieved calibration accuracies to the 20%–30% level, our study provides the first complete, medium-resolution, far-infrared spectrum, with substantially reduced uncertainty ($\sim 5\%$), no atmospheric problems, a standard aperture, and a single calibration scheme. Furthermore, by using line ratios rather than absolute fluxes to determine starburst/photodissociation region (PDR) properties, most systematic uncertainties should cancel.

4. MODELING AND OTHER RESULTS

4.1. Blackbody Fitting

We fit our spectrum with a function of the form $F_\lambda \propto B_\lambda(T)(1 - e^{-\tau_{\text{Dust}}})$, where we assume $\tau_{\text{Dust}} \propto \lambda^{-1}$. This gave us a good fit for a temperature of 48 K for the emitting dust.

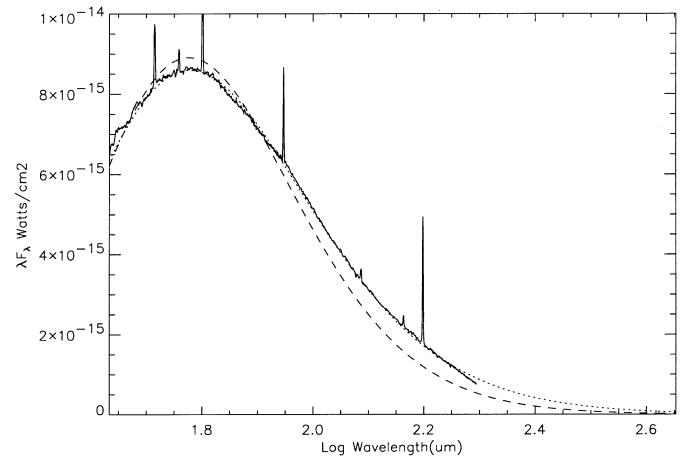


FIG. 2.—Blackbody fit. The solid line is actual data corrected for predicted extinction; the dotted line is a best-fit blackbody spectrum with flux density $\propto B_\lambda(T)(1 - e^{-\tau_{\text{Dust}}})$ law, where $\tau \propto \lambda^{-1}$. For comparison, the dashed line is our best fit with $\tau \propto \lambda^{-2}$.

If we then assume $\tau_{\text{Dust}} = 1$ at $\sim 2 \mu\text{m}$ (from $A_V = 10$), we get a covering fraction of almost unity. Emissivity laws where $\tau \propto \lambda^{-1.5}$ and λ^{-2} were also considered. The $\lambda^{-1.5}$ law does not fit as well, and the λ^{-2} law showed large deviations. The 48 K temperature is consistent with the formula from Spinoglio et al. (1995), which determines the color temperature of a galaxy with a λ^{-1} emissivity law from its spectral index found using only the flux densities at 60 and 100 μm . From our data α_{60-100} for M82 is 0.04. When we substitute that into their regression formula, $T_{\text{color}} = 11.4 \times (\alpha_{60-100} + 4.67)$ K, the result is 53 K, only 5 K different than a fit to the entire far-infrared spectrum.

Figure 2 shows the fit with extrapolation into the submillimeter. Not shown is Hughes, Gear, & Robson's (1994) data point for 450 μm , $\lambda F_\lambda = (2.7 \pm 0.4) \times 10^{-17} \text{ W cm}^{-2}$, measuring the flux from the central $68'' \times 68''$ of M82. Inputting 450 μm into our fit gives a $\lambda F_\lambda = 5.5 \times 10^{-17} \text{ W cm}^{-2}$, a factor of 2 high, indicating, perhaps, a steepening in the λ dependence for the dust emissivity law in the submillimeter. Klein, Wielebnski, & Morsi (1988), fitting a few points from the infrared, submillimeter, and out into the millimeter radio portion of the spectrum, did derive a steeper dust emissivity law, with $\tau_{\text{Dust}} \propto \lambda^{-1.5}$.

The total flux for the infrared region observed is $8.15 \times 10^{-15} \text{ W cm}^{-2}$, which at a distance of 3.63 Mpc corresponds to $3.2 \times 10^{10} L_\odot$. Assuming it continues short-

TABLE 2
KAO CONTINUA AND FLUXES

Line	KAO Line ^a (W cm ⁻²)	KAO Continuum (Jy)	HPBW (arcsec)	Reference
[O III] 52 μm	$9.5 \pm 0.7 \times 10^{-18}$	1207	48	1
[N III] 57 μm	$3.9 \pm 0.4 \times 10^{-18}$	1269	48	1
[O I] 63 μm	$14.2 \pm 3.4 \times 10^{-18}$	1254	44	2
[O III] 88 μm	$8.6 \pm 0.5 \times 10^{-18}$	1689	48	1
[N II] 122 μm	$2.9^{+0.9}_{-0.6} \times 10^{-18}$	1190	45	3
[O I] 145 μm	$0.84 \pm 0.24 \times 10^{-18}$	1130	55	4
[C II] 158 μm	$14 \pm 4.2 \times 10^{-18}$	1150	55	4

^a All line fluxes have been corrected for same extinction used in Table 1.

REFERENCES—(1) Duffy et al. 1987; (2) Lord et al. 1996; (3) Petuchowski et al. 1994; (4) Lugten et al. 1986.

ward of $43 \mu\text{m}$ as a blackbody, the total far-infrared flux would be $9.7 \times 10^{-15} \text{ W cm}^{-2}$ or $3.8 \times 10^{10} L_{\odot}$, in agreement with the estimate by Telesco & Harper (1980). The total flux in the fine structure lines is $6.0 \times 10^{-17} \text{ W cm}^{-2}$ or 0.6% of the infrared flux. The $[\text{C II}]/F(\text{FIR})$ ratio in the LWS beam is 1.4×10^{-3} , similar to that seen toward galactic H II regions and other starburst and normal galaxies (Stacey et al. 1991).

4.2. Emission-Line Ratio Modeling

A realistic starburst of a given age and duration is intermediate between the simple cases of an instantaneous burst and continuous star formation. In order to limit the number of free parameters and to bracket the real situation, we looked at two different starburst types, instantaneous burst and continuous star formation. For each one our combined starburst H II region and photodissociation region (PDR) model has six free parameters: density in H II region, density in PDR, ionization parameter in H II region, far-ultraviolet flux in PDR, input starburst age, and input starburst upper mass limit.

Table 3 lists the measured line ratios of M82 together with the predicted combination starburst (H II region) and PDR model ratios. Following the methodology of Fischer et al. (1996), the H II region model was created using the program CLOUDY by Gary Ferland (Version 90; Ferland 1996) and input spectral energy distributions (SEDs) of starbursts described in Leitherer & Heckman (1995). To test different SED models, we tried two upper cutoff masses, 30 and $100 M_{\odot}$, and two burst types, instantaneous bursts and continuous star formation, for ages of 1–25 Myr. All the SED models had solar metallicity and initial mass function (IMF) slopes of 2.35. The input parameters are density and the ionization parameter, U , which is defined as the ratio of ionizing photons to hydrogen atoms at the inner face of the cloud:

$$U = \frac{Q(H)}{4\pi r^2 n_{\text{H}} c}, \quad (1)$$

where $Q(H)$ is the number of (ionizing photons) s^{-1} , n_{H} is the total hydrogen density at the inner face of the cloud, and r is the distance from the ionizing source. Orion abundances

and dust grains were assumed for the emitting H II regions. The $[\text{O III}] 52 \mu\text{m}/[\text{O III}] 88 \mu\text{m}$ ratio is sensitive to density, but it is almost completely independent of ionization parameter and model type. We found the best fit for a density of 250 cm^{-3} for all models. The $[\text{N III}] 57 \mu\text{m}/[\text{N II}] 122 \mu\text{m}$ ratio acts in an orthogonal manner to our first diagnostic ratio. It is weakly dependent on density for low-density H II regions, but it is strongly dependent on ionization parameter and weakly dependent on model type. Here we fit $\log U$ varying from -3.1 for the $30 M_{\odot}$ cutoff continuous star formation to -3.5 for a 3–7 Myr old instantaneous burst with a $100 M_{\odot}$ cutoff. These fits with different ionization parameters demonstrate Spinoglio & Malkan's (1992) point that a harder ionizing spectrum can be somewhat compensated for by a modest decrease in U .

Change in input abundances made little difference in our derived starburst parameters. We ran CLOUDY models with Orion abundances, ISM abundances, solar abundances, and twice solar metallicity starburst abundances, where the abundances are those defined in CLOUDY (except for the ISM abundances, which come from Sembach & Savage 1996). No matter what abundances we input, we always derived basically the same densities and ionization parameters. The quality of the fit did vary somewhat, but this was mainly the fit of oxygen to nitrogen line ratios ($[\text{O III}] 52 \mu\text{m}/[\text{N III}] 57 \mu\text{m}$, $[\text{O III}] 88 \mu\text{m}/[\text{N II}] 122 \mu\text{m}$, and so on), which one would expect to change when altering the ratio of oxygen to nitrogen abundances. Orion abundances fit best, matching to within 10% of our measured ratios. ISM and solar abundances have only slightly different O/N abundance ratios, and so they also produced satisfactory fits (within 30%) of the measured O/N line ratios. Twice solar metallicity starburst abundances have high O/N abundance ratios and consequently produced high O/N line ratios, $\sim 2.5 \times$ that observed.

Of the four model input starburst SEDs considered, only two produced satisfactory ratio fits: the 3–7 Myr instantaneous burst with $100 M_{\odot}$ cutoff and the 8–25 Myr continuous star formation with $30 M_{\odot}$ cutoff. A fit was also achieved with the continuous star formation with $100 M_{\odot}$ cutoff, but only after reducing the nitrogen abundance by a third. We can further constrain the models by looking at their total bolometric luminosity. Using the extinction-

TABLE 3
LINE RATIOS

Line Ratio	Measured Ratio	Instantaneous ^a	Continuous ^b
$[\text{O III}] 52 \mu\text{m}/[\text{N III}] 57 \mu\text{m} \dots\dots$	3.0 ± 0.4	3.0	3.1
$[\text{O III}] 52 \mu\text{m}/[\text{O III}] 88 \mu\text{m} \dots\dots$	1.24 ± 0.08	1.26	1.32
$[\text{O III}] 52 \mu\text{m}/[\text{O I}] 63 \mu\text{m} \dots\dots\dots$	0.59 ± 0.04	0.59	0.59
$[\text{O III}] 52 \mu\text{m}/[\text{N II}] 122 \mu\text{m} \dots\dots$	6.3 ± 0.5	6.3	6.6
$[\text{O III}] 52 \mu\text{m}/[\text{O I}] 145 \mu\text{m} \dots\dots$	9.4 ± 0.9	9.2	10.5
$[\text{O III}] 52 \mu\text{m}/[\text{C II}] 158 \mu\text{m} \dots\dots$	0.82 ± 0.04	0.82 ^c	0.82 ^c
$[\text{N III}] 57 \mu\text{m}/[\text{N II}] 122 \mu\text{m} \dots\dots$	2.1 ± 0.3	2.1	2.1
$[\text{O I}] 63 \mu\text{m}/[\text{O I}] 145 \mu\text{m} \dots\dots\dots$	15.9 ± 1.4	15.5	17.9
$[\text{O I}] 63 \mu\text{m}/[\text{C II}] 158 \mu\text{m} \dots\dots\dots$	1.38 ± 0.03	1.39	1.41
$[\text{N II}] 122 \mu\text{m}/[\text{N II}] 205 \mu\text{m} \dots\dots$	$4.1 \pm 1.4^{\text{d}}$	4.4	4.9

^a Instantaneous burst model, 3–5 Myr old with $100 M_{\odot}$ cutoff plus PDR contribution, the preferred model.

^b Continuous star formation model, 8–25 Myr old with $30 M_{\odot}$ cutoff plus PDR contribution. This model was rejected, because it produced too much luminosity.

^c This ratio is forced to match exactly by the fitting method.

^d ISO did not observe the $[\text{N II}] 205 \mu\text{m}$ line; we use the KAO observation from Petuchowski et al. (1994).

corrected $\text{Br}\gamma$ flux contained within an *ISO* LWS beam (from Satyapal et al. 1997) and assuming an electron density $\sim 200 \text{ cm}^{-3}$ and an electron temperature $\sim 5000 \text{ K}$, we found an ionizing photon rate of $8 \times 10^{53} \text{ s}^{-1}$. This is similar to values previously found. For instance, McLeod et al. (1993) found a rate of $1.05 \times 10^{54} \text{ s}^{-1}$ using a smaller beam ($30''$) but different assumptions about extinction. As one experiment, we scaled the Leitherer & Heckman (1995) models to this ionizing photon rate and found that the continuous star formation produces $\sim 10^{11} L_{\odot}$, more than twice the measured far-infrared luminosity ($\sim 4 \times 10^{10} L_{\odot}$). The older instantaneous bursts also produce too much luminosity, but the more recent bursts, 3–5 Myr old, only produce $(3\text{--}5) \times 10^{10} L_{\odot}$, more consistent with the observed total far-infrared luminosity. This makes the 3–5 Myr instantaneous burst our preferred input SED. Small errors in ionizing photon rate do not affect this conclusion.

A similar check was made by comparing the Leitherer & Heckman (1995) starburst masses expected to the dynamical mass derived from the mass model by Gotz et al. (1990), which gives us $1.6 \times 10^9 M_{\odot}$ within our *ISO* beam. McLeod et al. (1993) also used the Gotz et al. (1990) mass model but for their smaller beam size. After they subtracted estimates for molecular mass and an older stellar population, they arrived at an estimate of $2.5 \times 10^8 M_{\odot}$ for the starburst population. Rieke et al. (1993) used this mass limit along with modeling to predict that a lower mass cutoff must exist. Our preferred instantaneous burst model predicts starburst masses of $0.5\text{--}1.3 \times 10^8 M_{\odot}$, depending on lower mass cutoff ($1.0\text{--}0.1 M_{\odot}$), which does not come close to exceeding the dynamical mass contained within the *ISO* beam. Even if we take the $2.5 \times 10^8 M_{\odot}$ used by Rieke et al. (1993) as our total allowed starburst mass, we have no trouble fitting the mass and see no requirement for a lower mass cutoff, although one might possibly exist.

While the *CLOUDY* models fit the starburst lines well, they produce little $[\text{O I}]$ and $[\text{C II}]$ line emission. The amount of $[\text{C II}]$ $158 \mu\text{m}$ line flux produced by the *CLOUDY* models depends on the SED we input, but it is $\sim 24\%\text{--}31\%$ of the total observed line flux for the instantaneous burst. Both $[\text{C II}]$ and $[\text{O I}]$ lines are strongly produced in PDRs, which one would expect to find in the interface between H II regions and molecular clouds. We use the PDR models of Kaufman et al. (1998). These models have two free parameters: density and far-ultraviolet flux, G_0 , which is expressed in units of local Galactic far-ultraviolet flux, or $1.6 \times 10^{-3} \text{ ergs s}^{-1} \text{ cm}^{-2}$. Once again the line ratios provide excellent diagnostics for determining these parameters. The ratio of $[\text{O I}]$ $63 \mu\text{m}/[\text{O I}]$ $145 \mu\text{m}$ acts orthogonally to the $[\text{O I}]$ $63 \mu\text{m}/[\text{C II}]$ $158 \mu\text{m}$ ratio over the densities and far-ultraviolet fluxes considered (Wolfire, Tielens, & Hollenbach 1990). If we assume that the remaining $69\%\text{--}76\%$ of the $[\text{C II}]$ not accounted for by the starburst H II region model is coming from the PDRs, then we have our PDR $[\text{O I}]$ $63 \mu\text{m}/[\text{C II}]$ $158 \mu\text{m}$ ratio of $\sim 1.6\text{--}1.8$. Combining that with the observed $[\text{O I}]$ $63 \mu\text{m}/[\text{O I}]$ $145 \mu\text{m}$ ratio (~ 16) gives us a density of $10^{3.3} \text{ cm}^{-3}$ and a G_0 around $10^{2.8}$. These combined H II region and PDR models fit not only the line ratios, but, scaled to the distance and size of M82, they also fit the lines and continuum seen.

We can check our derived G_0 and PDR density using another PDR diagnostic, the ratio of the PDR line fluxes to the infrared continuum flux. For our parameters the

Kaufman et al. (1998) models give $\text{Flux}(\text{C II } 158 \mu\text{m} + \text{C II } 63 \mu\text{m} + \text{O I } 145 \mu\text{m})/\text{FIR} = 3.9 \times 10^{-3}$, roughly equal to the 2.9×10^{-3} we get after subtracting our H II region line contribution. It should be noted that the Kaufman et al. (1998) PDR models use Galactic ISM abundances, not the Orion abundances input into our *CLOUDY* H II region models. However, for our PDR density and G_0 , the difference in using two different abundances is negligible.

Since the regions we are modeling are in physical contact with one another, we should be able to make some continuity checks across the model boundaries. Following the treatment described by Satyapal et al. (1998), we start by checking that there is pressure equilibrium between the H II region and the PDR. The edge of the H II region has a temperature of 4000 K , which gives a $P/k \sim 10^6 \text{ cm}^{-3} \text{ K}$. Inputting our PDR surface temperature of $\sim 250 \text{ K}$, derived from Kaufman et al. (1998), and density gives a $P/k \sim 5 \times 10^5 \text{ cm}^{-3} \text{ K}$ or roughly the same as our H II region. The second boundary condition is that the far-ultraviolet flux leaving the H II region should equal that entering our PDR model. We measure the far-ultraviolet flux leaving the H II region by taking the *CLOUDY* output continuum and integrating the flux from 6 to 13 eV. This depends strongly on input SED, giving us $G_0 = 10^{2.2}\text{--}10^{2.4}$ for the instantaneous burst models. Considering the uncertainties, this is consistent with our model $G_0 = 10^{2.8}$.

Lester et al. (1987) noted that the $[\text{O III}]$ $52 \mu\text{m}/[\text{N III}]$ $57 \mu\text{m}$ ratio will equal the actual $\text{O}^{++}/\text{N}^{++}$ ratio within $\pm 50\%$, thanks to the similar critical densities for thermalization of their respective emitting levels and ionization potentials, which are within 25% of each other. With knowledge of the electron density, which one can get accurately from the $[\text{O III}]$ $52 \mu\text{m}/[\text{O III}]$ $88 \mu\text{m}$ ratio, a very precise $\text{O}^{++}/\text{N}^{++}$ ratio can be found that holds true for a broad range of electron temperatures. Following the calculations of Lester et al. (1987) and taking our density of 250 cm^{-3} , we find a $\text{O}^{++}/\text{N}^{++}$ ratio of 3.8. This is slightly higher than that reported by Duffy et al. (1987) for M82, $\text{O}^{++}/\text{N}^{++} = 3.1$. Both ratios are higher than the average value of H II regions toward the Galactic center, where $\langle \text{O}^{++}/\text{N}^{++} \rangle \sim 0.9\text{--}1.4$ (Dinerstein et al. 1984). One possible conclusion that could be drawn is that the O/N ratio is truly higher in M82. However, it is more likely that this is an effect of the local ionizing conditions. In low-ionization conditions, i.e., cool stars, more nitrogen is doubly ionized than oxygen, because the ionization potential of N^+ is smaller than that of O^+ . The difference in $\text{O}^{++}/\text{N}^{++}$ ratio in the Galaxy would result from less massive (cooler) stars creating the H II regions. This is further supported by our model fit, where we fit the O^{++} and N^{++} lines for M82 with a high-ionization starburst SED and Orion abundances without any oxygen overabundance. In fact, as this section mentioned earlier, the more oxygen-rich abundance models produced significantly worse fits to our line ratios.

Examining our best fit we come within 10% of all the ratios and closer on most. The derived parameters—H II region density, PDR density, ionization parameter, far-ultraviolet flux, burst upper mass cutoff, and burst age—are well determined, with even small changes in any of these inputs creating ratios outside the uncertainties of the ratios measured. The majority of error still present in these fits comes from the models themselves and the assumptions we made, not from the inaccuracy in our line ratio measurements.

We can compare this work with previous models. Spinoglio & Malkan (1992) also fit far-infrared lines with a combination H II region and PDR model. While achieving similar H II region densities, their M82 model had a much larger ionization parameter ($10^{-2.5}$). This is entirely due to the hardness of the input SED. The Leitherer & Heckman (1995) SEDs are significantly harder than the SED Spinoglio & Malkan (1992) used. The Spinoglio & Malkan (1992) PDR parameters were also different ($G_0 = 10^4$, $n = 10^{4-5} \text{ cm}^{-3}$), but this can be mainly attributed to the newer PDR models of Kaufman et al. (1998). The Lord et al. (1996) PDR parameters for M82 ($G_0 = 10^3$, $n = 10^4 \text{ cm}^{-3}$) come closer to our derived values, but they also differ because of the newer models used.

Satyapal et al. (1997) and Reike et al. (1993) previously created models of the M82 starburst, both finding typical starburst ages of around 10^7 yr. Reike et al. (1993) compared many observational parameters (M_K , mass, luminosity, CO index, UV photons), fitting M82 with two separate starbursts, the first being 13–30 Myr ago. Satyapal et al. (1997) looked at individual starburst clusters, measuring their CO indices and Br γ equivalent widths. Modeling those features for each individual cluster, they found a range in age of 6×10^6 yr, implying an outward propagating starburst. For the sake of simplicity, we did not attempt to combine multiple models with different starburst ages, but we note many of the individual starburst cluster ages found by Satyapal et al. (1997) were around 5 Myr.

One unknown that could throw off the models is the degree of [O I] 63 μm self-absorption in M82. Stacey et al. (1983) first observed the 145 μm [O I] line from the PDR associated with the Orion A H II region and discovered that the [O I] 63, 145, and [C II] 158 μm line intensity ratios indicated optically thick ($\tau \sim 2$) emission in the 63 μm line. Tielens & Hollenbach (1985) models also indicated that this should be so. Later, through more sophisticated modeling involving the [¹³C II] line and more complete mapping in the [C II] and [O I] lines, Stacey et al. (1993) estimated that the [O I] 63 μm has an optical depth ~ 3 in the Orion PDR. The [O I] 63 μm line is seen in absorption in Arp 220 (Fischer et al. 1998) and in Galactic star formation regions (Poglitsch et al. 1996; Baluteau et al. 1997). In addition, Hermann et al. (1997) explained an unusually low [O I] 63 μm /[O I] 145 μm ratio in the Dark Lane region of the Orion Molecular Cloud as a likely site of [O I] 63 μm self-absorption.

One would expect [O I] 63 μm absorption to occur where cold foreground oxygen lies between us and an emitting source. However, the gas density must exceed the critical density for collisional de-excitation ($n_{\text{crit}} \sim 5 \times 10^5 \text{ cm}^{-3}$) in order for the absorbed photons to be removed from our beam. At lower densities the photons are mainly scattered, with little reduction in the observed line luminosity. In our Galaxy, such dense clouds rarely cover more than a small fraction of the [O I]-emitting region. Since the ISM in most starburst and normal galaxies seems to be constructed of a superposition of many such clouds, which usually do not cover each other simultaneously in both velocity and area, the small regions of [O I] self absorption should not be important. A notable exception is Arp 220 (Fischer et al. 1998), where it is likely the FIR source is largely enveloped by cold, dense clouds with abundant neutral oxygen. There is no reason to think of M82 as such an extreme case, and in fact our analysis of high signal-to-noise ratio Fabry-Perot

scans of the [O I] 63 μm line does not indicate any self-absorption. Any significant [O I] self-absorption would alter the PDR modeling by increasing the PDR density.

There is one more important forbidden line in the far-infrared, the [N II] 205 μm line, which lies just beyond the LWS limit of 196.7 microns. Petuchowski et al. (1994) measured it using the KAO, and our model does predict its relative flux. We include both on our line ratio table and note they match to within the uncertainty of the KAO flux measurements. The [N II] line ratio is the best density tracer for low-density ($n < 500 \text{ cm}^{-3}$) H II regions, so the accurate reproduction of this line ratio lends credence to our estimate: $n_e \sim 250 \text{ cm}^{-3}$.

4.3. Cross Scans of the C II and O I Lines

In addition to the full scan made at the center of M82, we collected cross-scans of the [C II] 158 and [O I] 63 μm lines using the LWS02 Astronomical Observation Template (AOT). The maps consist of two cuts across M82, one across the major axis with a P.A. = 55° and the other across the minor axis, perpendicular to the first. Seven observations were made in each cut, starting 150" from M82's center and spaced 50" apart. Each line represents an integration of 3 s (spectral element)⁻¹. The two plots in Figure 3 show the relative strengths of the emission lines along the two axes. Only upper limits were found for the [O I] 63 μm line at the points 150" from M82's center and are therefore not included on the map. The major axis cut runs from southwest to northeast, and the minor axis cut runs from northwest to southeast.

Both lines weaken away from the center, but while the [C II] 158 μm line fall-off is symmetrical about the minor axis, it is not symmetrical about the major axis; the [O I] 63 μm line is not symmetrical around either axis. This asymmetry is not that surprising. Previous maps, such as those in H α (Waller, Gurwell, & Tamura 1992), the near-infrared (Satyapal et al. 1995), and the submillimeter (Hughes et al. 1994), show an excess in flux to the west. Stacey et al. (1991)

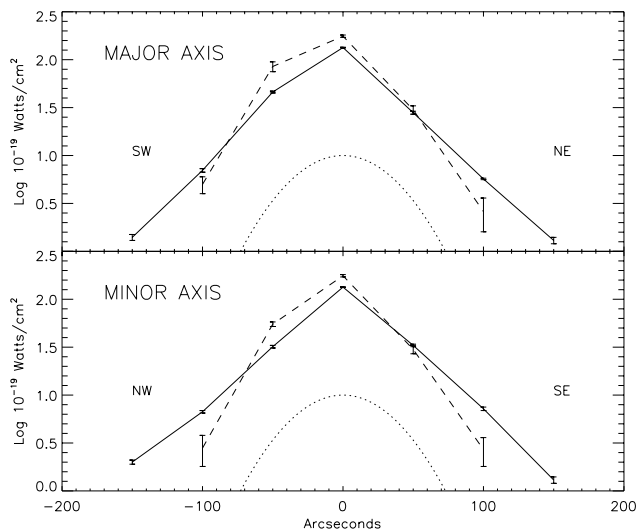


FIG. 3.—Plots of the strengths of two lines across the major (top) and minor (bottom) axis of M82. The solid line is the [C II] 158 μm line, and the dashed line is the [O I] 63 μm line. The LWS beam is represented by the dotted line.

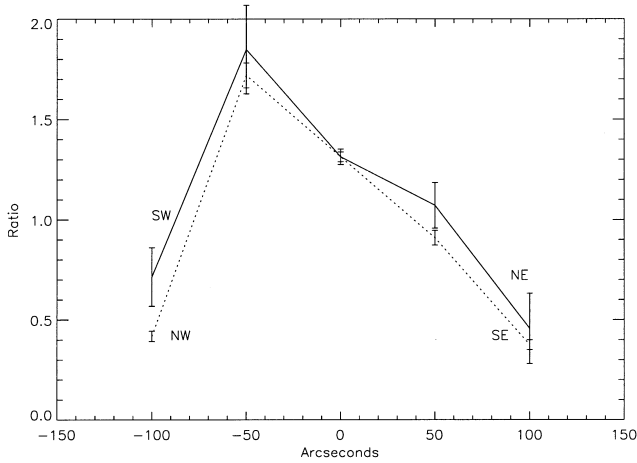


FIG. 4.—Plot of $[\text{O I}]/[\text{C II}]$ line ratio across M82. The solid line is the ratio across the major axis, and the dotted line is the ratio along the minor axis.

did similar cuts in the $[\text{C II}]$ $158 \mu\text{m}$ line, which also showed this slight asymmetry in the major axis. Lord et al. (1996) did detailed modeling of $[\text{O I}]$ $63 \mu\text{m}$ line profile, attributing the majority of the line flux to two off-center hot spots, with the western spot the brighter of the two. We examined the far-infrared continuum in our cross scans and also found more flux to the west.

We measured the spectral index α between 60 and $100 \mu\text{m}$, where $F_\nu \propto \nu^\alpha$, at every spot in our scans. This α_{60-100} is largest $50''$ to the west, where it is ~ 0.4 , not at M82's center, where α_{60-100} is ~ 0.1 . This higher α_{60-100} implies a higher average temperature, further indication of a strong hot spot to the west. In addition, we also looked at the spectral index α between 100 and $175 \mu\text{m}$, where we were interested in testing whether our single temperature blackbody with emissivity $\propto \lambda^{-1}$ would fit further outward from the galaxy's center. The $\alpha_{100-175}$ at the hot spot to the west is ~ 1.6 , which is consistent with our blackbody fit. However, the $\alpha_{100-175}$ measured to the east and farther outward in the galaxy is smaller than expected, possibly indicating a growing cold dust component.

Most interesting is the variation in the $[\text{O I}]$ $63 \mu\text{m}/[\text{C II}]$ $158 \mu\text{m}$ line ratio, visible in Figure 4. Assuming the two lines come mostly from PDRs, tracing the $[\text{O I}]$ $63 \mu\text{m}/[\text{C II}]$ $158 \mu\text{m}$ line ratios will tell us something about conditions in M82 on a large scale. The ratio shows a maximum roughly $50''$ off center to the northwest and southwest of the galaxy's center and shows a steady decrease outward. According to the models of Kaufman et al. (1998), this ratio decreases with PDR density and far-ultraviolet field strength. The general trend of decreasing $[\text{O I}]$ $63 \mu\text{m}/[\text{C II}]$ $158 \mu\text{m}$ ratio with distance from M82's center is then understandable. One would expect both density and far-ultraviolet field to decrease with distance from the galaxy's center. The off-center maximum in the $[\text{O I}]$ $63 \mu\text{m}/[\text{C II}]$ $158 \mu\text{m}$ ratio must indicate where conditions of high density, high G_0 , or both exist.

The $[\text{C II}]$ $158 \mu\text{m}$ line flux also appears more extended than the $[\text{O I}]$ $63 \mu\text{m}$ line flux, possibly indicating its association with the filamentary features observed in optical recombination lines, as previously suggested by Stacey et al. (1991). Taking the formula for $[\text{C II}]$ intensity originating

from ionized regions from Madden et al. (1993), we get

$$I_{\text{C}^+}(\text{ionized}) = \frac{h\nu}{4\pi} \frac{A}{n_{\text{crit}}} \frac{g_u/g_l}{1 + [(g_u/g_l) + 1](n_e/n_{\text{crit}})} X_{\text{C}^+} \text{EM}, \quad (2)$$

where A is the spontaneous emission coefficient for the ${}^2P_{3/2} - {}^2P_{1/2}$ transition ($2.36 \times 10^{-6} \text{ s}^{-1}$), g_u/g_l is the ratio of statistical weights in the upper and lower levels (2), n_{crit} is the critical density ($\sim 35 \text{ cm}^{-3}$), X_{C^+} is the abundance of C^+ relative to hydrogen ($\sim 3.3 \times 10^{-4}$), and EM is the emission measure. Assuming electron density is low compared to the critical density, we only need a measurement of the emission measure to derive the expected flux from the extended, diffuse ionized gas of M82. We derive the EM from the 6 cm maps of Seaquist & Odegard (1991), assuming the majority of the emission comes from thermal free-free emission. At roughly $50''$ off the minor axis we find an EM $\sim 1300 \text{ cm}^{-6} \text{ pc}$, giving us an expected intensity for C^+ of $1.7 \times 10^{-4} \text{ ergs s}^{-1} \text{ cm}^{-2} \text{ sr}^{-1}$ or an expected flux in our ISO LWS beam of $2.0 \times 10^{-18} \text{ W cm}^{-2}$. This number is consistent with that observed, indicating that the majority of the extended C^+ emission is coming from the diffuse ionized medium.

4.4. OH absorption

The only certain absorption feature observed in the spectrum of M82 is due to the two lambda-doubling rotational transitions of OH at $\sim 119.4 \mu\text{m}$, which are unresolved at the LWS grating-mode resolution. These are the transitions from the OH ground state of ${}^2\pi_{3/2} J = 3/2$ to the next highest energy state, ${}^2\pi_{3/2} J = 5/2$, which have been seen before in emission in the KL nebula (Storey, Watson, & Townes 1981) and in absorption toward the Galactic center (Genzel et al. 1985). No other OH lines are observed in M82. There is a dip at the location of the $53 \mu\text{m}$ transitions, but it is the same scale as the noise and must be treated as an upper limit. Table 4 lists the 1σ upper limits for the next most likely OH lines.

The equivalent width of an optically thin line is

$$W = A_{ij} \frac{g_i}{g_j} \frac{\lambda_0^4}{8\pi c} N, \quad (3)$$

where A_{ij} is the Einstein coefficient for spontaneous emission between two levels, i and j ; g is their statistical weights; λ_0 is the transition's line center; and N is the column density of material (Aller 1960). Taking the A coefficients from Destombes et al. (1977), one can calculate column densities and column density upper limits for the lines. Three of the transitions, 53, 79, and $119 \mu\text{m}$, are all from the ground state, but we only detect the $119 \mu\text{m}$ line because the A -coefficients for 53 and $79 \mu\text{m}$ give equivalent widths 20–80 times less than that of the $119 \mu\text{m}$ transition, assuming the

TABLE 4
OH LINES

Line (μm)	Transition	Equivalent Width (μm)	A_{ij} (s^{-1})
53	${}^2\pi_{3/2} J = 3/2 \rightarrow \pi_{1/2} 2 J = 3/2$	<0.003	0.04
79	${}^2\pi_{3/2} J = 3/2 \rightarrow \pi_{1/2} 2 J = 1/2$	<0.004	0.033
84	${}^2\pi_{3/2} J = 5/2 \rightarrow \pi_{3/2} 2 J = 7/2$	<0.004	0.5
119	${}^2\pi_{3/2} J = 3/2 \rightarrow \pi_{3/2} 2 J = 5/2$	0.022 ± 0.004	0.13
163	${}^2\pi_{1/2} J = 1/2 \rightarrow \pi_{3/2} 2 J = 3/2$	<0.005	0.054

transitions are optically thin. This is consistent with the upper limits observed. The lack of the 84 and 163 μm lines, despite having higher cross sections, demonstrates that the absorbing OH gas is almost entirely in its ground state. The column density of OH in its ground rotational state is $\sim 4.2 \times 10^{14} \text{ cm}^{-2}$. Further analysis will be presented in a later paper.

Besides the 119 μm OH absorption lines and the seven emission lines, we identify no other lines or other features in the spectrum. We should, however, point out some visible features in the spectrum that may or may not be real. The large bumps at the shortest wavelengths, 43–50 μm , are present in other LWS spectra (Arp 220; Fischer et al. 1998). These features appear to be an artifact of that detector, SW1, but they are being investigated further. Two other apparent features at 56 and 112 μm , result from unexpected HD lines in the Uranus calibration spectrum. The 56 μm line is particularly troublesome, because it confuses the situation on the short wavelength side of the [N III] 57 μm line, where there is a hint of an absorption, possibly a $p\text{-H}_2\text{O}$ line. Harvey et al (1998) have examined the ISO/LWS M82 spectrum for evidence of atomic hydrogen recombination lines in this range. None were detected. The upper limits, constrained by their very low line-to-continuum ratio, lie within the range of expected values set by the known centimeter and decimeter lines and a spontaneous emission process. Other potential features not already mentioned are absorptions at 65.1, 66.4, and 149.2 μm . Further analysis and possible identification will come in a later paper. Any undetected lines present in the M82 spectrum would have to have fluxes less than $\sim 5 \times 10^{-19} \text{ W cm}^{-2}$ at 50 μm to $\sim 2 \times 10^{-19} \text{ W cm}^{-2}$ at 180 μm .

5. CONCLUSIONS

We have obtained an LWS full grating scan of the prototypical starburst galaxy, M82. This spectrum reveals seven bright fine structure lines, previously detected from the KAO but here detected at the same time, with the same instrument, with roughly the same beam, and without any

obstructing atmosphere. Therefore, the relative calibration of these lines is superior to that used for prior analysis. Also reported is the discovery of an absorption line of OH from its lowest state. The upper limits for other possible OH lines are enough to determine that most of the absorbing OH is in its ground state. The whole spectrum is well fitted by a single temperature dust component with an optical depth $\tau_{\text{Dust}} \propto \lambda^{-1}$, giving a total infrared flux of $3.8 \times 10^{10} L_{\odot}$.

We fitted the infrared line ratios of M82 with a six-parameter combination H II region and PDR model. The parameters for the best fitting model are H II region density = 250 cm^{-3} , $U = 10^{-3.5}$, PDR density = $10^{3.3} \text{ cm}^{-3}$, $G_0 = 10^{2.8}$, upper mass cutoff = 100 M_{\odot} and age = 3–5 Myr. The [C II] 158 μm line comes $\sim 25\%$ from the H II regions and $\sim 75\%$ from PDRs. In our model, the starburst mass is $\sim (0.5\text{--}1.3) \times 10^8 M_{\odot}$, depending on the lower mass cutoff chosen. This is a significant percentage of the molecular mass ($\sim 2 \times 10^8 M_{\odot}$, Wild et al. 1992), indicating the M82 starburst will not be able to continue producing stars, through another instantaneous burst or otherwise, for much longer before running out of mass. The LWS cross-scan data support the model of strong, off-center hot spots seen in the mid-infrared (Telesco et al. 1991) and modeled from velocity profiles by Lord et al. (1996). Our fit for a 3–5 Myr instantaneous starburst is a simplification of the true situation, which is several regions with different starburst ages. The single burst we modeled should be dominated by the brightest and most recent bursts, which are presumably the hot spots themselves.

This work was made possible by the hard work and dedication of the ISO team and the LWS consortium. We gratefully acknowledge the use of the Kaufman et al. (1998) models. In particular we would like to thank Matt Greenhouse, Mark Wolfire, and Michael Kaufman for their comments and help. This work was supported by the NASA ISO program, including NASA grants NAG 5-3309, NAGW-1711, and NAGW-4038. J. F. and M. L. also acknowledge support by the Office of Naval Research.

REFERENCES

- Adams, F. C., Lada, C. J., & Shu, F. H. 1988, *ApJ*, 326, 865
 Aller, L. H. 1960, *Stellar Atmospheres*, ed. Greenstein, J. L. (Chicago: Univ. Chicago Press), 156
 Baluteau, J. -P., et al. 1997, *A&A*, 322, L33
 Clegg, P. E., et al. 1996, *A&A*, 315, L38
 Destombes, J. L., Marliere, C., Baudry, A., & Brillet, J. 1977, *A&A*, 60, 55
 Dinerstein, H. L., Lester, D. F., Werner, M. W., Watson, D. M., Genzel, R., & Rubin, R. 1984, in *Airborne Astronomy Symposium Proceedings*, ed. H. A. Thronson and E. F. Erickson (NASA CP: 2353), 266
 Duffy, P. B., Erickson, E. F., Haas, M. R., & Houck, J. R. 1987, *ApJ*, 315, 68
 Ferland, G. J. 1996, *Univ. Kentucky Dept. Phys. Astron. Int. Rep.*
 Fischer, J., et al. 1998, in *First ISO Workshop on Analytical Spectroscopy*, ed. A. M. Heras, K. Leech, N. R. Trams, & M. Perry (Noordwijk: ESA), 149
 ———, 1996, *A&A*, 315, L97
 Freedman, W., et al. 1994, *ApJ*, 427, 628
 Genzel, R., et al. 1998, *ApJ*, 498, 579
 Genzel, R., Watson, D. M., Crawford, M. K., & Townes, C. H. 1985, *ApJ*, 297, 766
 Gotz, M., McKeith, C. D., Downes, D., & Greve, A. 1990, *A&A*, 240, 52
 Harvey, V. I., Satyapal, S., Smith, H. A., and Strelitski, V. 1998, *AJ*, submitted
 Herrmann, F., Madden, S. C., Nikola, T., Poglitsch, A., Timmerman, R., Geis, N., Townes, C. H., & Stacey, G. J. 1997, *ApJ*, 481, 343
 Hughes, D. H., Gear, W. K., & Robson, E. I. 1994, *MNRAS*, 270, 641
 Kaufman, M., Wolfire, M., Hollenbach, D., & Luhman, M. 1998, in *Preparation*
 Kenney, J. D. P., Wilson, C. D., Scoville, N. Z., Devoreux, N. A., & Young, J. S. 1992, *ApJ*, 395, L79
 Kessler, M. F., et al. 1996, *A&A*, 315, L27
 Klein, U., Wielebinski, R., & Morsi, H. W. 1988, *A&A*, 190, 41
 Leitherer, C., & Heckman, T. M. 1995, *ApJS*, 96, 9
 Lester, D. F., Dinerstein, H. L., Werner, M. W., Watson, D. M., Genzel, R., & Storey, J. W. V. 1987, *ApJ*, 320, 573
 Lord, S. D., Hollenbach, D. J., Haas, M. R., Rubin, R. H., Colgan, S. W. J., & Erickson, E. F. 1996, *ApJ*, 465, 703
 Lugten, J. B., Watson, D. M., Crawford, M. K., & Genzel, R. 1986, *ApJ*, 311, L51
 Madden, S. C., Geis, N., Genzel, R., Herrmann, F., Jackson, J., Poglitsch, A., Stacey, G. J., & Townes, C. H. 1993, *ApJ*, 407, 579
 McLeod, K. K., Rieke, G. H., Rieke, M. J., & Kelly, D. M. 1993, *ApJ*, 412, 111
 Petuchowski, S. J., Bennett, C. L., Haas, M. R., Erickson, E. F., Lord, S. D., Rubin, R. H., Colgan, S. W., & Hollenbach, D. J. 1994, *ApJ*, 427, L17
 Poglitsch, A., Herrmann, F., Genzel, R., Madden, S. C., Nikola, T., Timmermann, R., Geis, N., & Stacey, G. J. 1996, *ApJ*, 462, L43
 Rieke, G. H., Loken, K., Rieke, M. J., & Tambllyn, P. 1993, *ApJ*, 412, 99
 Rice, W., Lonsdale, C. J., Soifer, B. T., Neugebauer, G., Kopan, E. L., Lloyd, L. A., DeJong, T., & Habing, H. J. 1988, *ApJS*, 68, 91
 Satyapal, S., Watson, D. M., Pipher, J. L., Forrest, W. J., Greenhouse, M. A., Smith, H. A., Fischer, J., & Woodward, C. E. 1997, *ApJ*, 483, 148
 Satyapal, S., et al. 1995, *ApJ*, 448, 611
 Satyapal, S., et al. 1998, in *Preparation*
 Seaquist, E. R., & Odegard, N. 1991, *ApJ*, 369, 320
 Sembach, K. R., & Savage, B. D. 1996, *ApJ*, 457, 211
 Spinoglio, L., & Malkan, M. A. 1992, *ApJ*, 399, 504
 Spinoglio, L., Malkan, M. A., Rush, B., Carrasco, L., & Recillas-Cruz, E. 1995, *ApJ*, 453, 616
 Stacey, G. J., Geis, N., Genzel, R., Lugten, J. B., Poglitsch, A., Sternberg, A., & Townes, C. H. 1991, *ApJ*, 373, 42
 Stacey, G. J., Jaffe, D. T., Geis, N., Genzel, R., Harris, A. I., Poglitsch, A., Stutzki, J., & Townes, C. H. 1993, *ApJ*, 404, 219

- Stacey, G. J., Smyers, S. D., Kurtz, N. T., & Harwit, M. 1983, *ApJ*, 265, 7
- Storey, J. W. V., Watson, D. M., & Townes, C. H. 1981, *ApJ*, 244, L27
- Swinyard, B. M., et al. 1998, in *Proc. SPIE*, 3354, in press
- Telesco, C. M., Campins, H., Joy, M., Dietz, K., & Decher, R. 1991, *ApJ*, 369, 135
- Telesco, C. M., & Harper, D. A. 1980, *ApJ*, 235, 392
- Tielens, A. G. G. M., & Hollenbach, D. 1985, *ApJ*, 291, 722
- Waller, W. H., Gurwell, M., & Tamura, M. 1992, *AJ*, 104, 63
- Watson, D. M., Genzel, R., Townes, C. H., Werner, M. W., & Storey, J. W. V. 1984, *ApJ*, 279, L1
- Wild, W., Harris, A. I., Eckart, A., Genzel, R., Graf, U. U., Jackson, J., Russell, A. P. G., & Stutzki, J. 1992, *A&A*, 265, 447
- Wolfire, M. G., Tielens, A. G. G. M., & Hollenbach, D. 1990, *ApJ*, 358, 116
- Yun, M. S., Ho, P. T., & Lo, K. Y. 1993, *ApJ*, 411, L17